

## Optimization of Perfusion CT Protocol for Imaging of Extracranial Head and Neck Tumors

Sotirios Bisdas,<sup>1</sup> Chuan Zhi Foo,<sup>2</sup> Choon Hua Thng,<sup>2</sup> Thomas J. Vogl,<sup>1</sup> and Tong San Koh<sup>3</sup>

The *in vivo* assessment of physiological processes associated with microcirculation in the head and neck tissue by means of perfusion computed tomography is widely used in the management of patients with head and neck tumors. However, there is no systematic consideration of the total acquisition duration and placement of the scans. A simulation study for optimizing perfusion studies of extracranial head and neck tumors, with considerations of reducing radiation dose while maintaining accuracy of the perfusion parameters, is demonstrated here. The suggested that dual-phase optimized protocols may provide reliable estimations of the permeability surface area product as well as blood flow and volume without additional radiation burden and serious patient discomfort. These optimized protocols can potentially be useful in the clinical setting of examining patients with extracranial head and neck tumors.

**KEY WORDS:** Perfusion CT, blood flow, blood volume, permeability surface-area product, head and neck

### INTRODUCTION

**D**ynamic contrast-enhanced (DCE) imaging using computed tomography (CT) or magnetic resonance imaging (MRI) has recently attracted much attention as it allows for non-invasive, *in vivo* assessment of physiological parameters such as blood flow, blood volume, transit time, and permeability.<sup>1-4</sup> Several studies have shown that the microcirculatory parameters derived using DCE imaging correlate with tumor histopathology indices and immunohistochemical surrogates of tumor neoangiogenesis.<sup>5-7</sup>

For analysis of DCE-CT data, the deconvolution approach which derives physiological parameters from the impulse residue function  $R(t)$  (where  $t$  denotes time) of the tissue has been increasingly used. The deconvolution method used also for the

calculation of permeability changes has been the method of choice in several reports in recent literature.<sup>8-10</sup> Although the acquisition time of DCE-CT data in these studies varies from 50–55 s, other variations in imaging protocols among these studies are apparent. The delay before the initiation of the contrast-enhanced scans can be up to about 6 s after contrast injection, and the injection rate is not standardized, which results in different durations of the contrast agent passage in the tissue microvasculature. Generally, modifications in the DCE-CT imaging protocol can be implemented depending on the organs or tissues imaged, and the physiological parameters of interest in the study.

Examining the effect of acquisition time in permeability imaging, Goh et al. showed interestingly that there are significant changes in permeability values between 45-, 65-, and 130-s examination protocols in colorectal cancer imaging.<sup>11</sup> However, in perfusion imaging of the brain to estimate cerebral blood flow and transit time, it is com-

<sup>1</sup>From the Department of Diagnostic and Interventional Radiology, Johann Wolfgang Goethe University Hospital, Theodor Stern Kai 7, 60590, Frankfurt, Germany.

<sup>2</sup>From the Department of Oncologic Imaging, National Cancer Center, Singapore, Singapore.

<sup>3</sup>From the School of Electrical and Electronic Engineering, Nanyang Technological University, Singapore, Singapore.

Correspondence to: Sotirios Bisdas, Department of Diagnostic and Interventional Radiology, Johann Wolfgang Goethe University Hospital, Theodor Stern Kai 7, 60590, Frankfurt, Germany; Tel: +49-69-63017260; Fax: +49-69-63015252; e-mail: s.bisdas@med.uni-frankfurt.de

Copyright © 2008 by Society for Imaging Informatics in Medicine

Online publication 3 May 2008

doi: 10.1007/s10278-008-9122-3

monly believed that duration of about 50 s could be adequate.<sup>12</sup> For DCE imaging of head and neck cancer, there is currently no available data pertaining to the optimal perfusion CT acquisition duration. In order to capture information on capillary-tissue exchange, one may need to increase the acquisition time (e.g. >55 s) in order to include the period when contrast is exchanged between intra- and extravascular spaces. However, the delayed imaging could increase the risk of motion-related artifacts and radiation-related side effects. Although the number of scans can be kept constant by increasing the scan interval to achieve delayed imaging, this compromise in temporal resolution could directly affect the accuracy of the estimated perfusion parameters.

In this work, we attempted to explore the optimal time placement of scans for DCE-CT imaging of head and neck carcinomas with the objectives of reducing radiation dose and examination duration, while not compromising on parameter estimation accuracy. A Monte Carlo simulation approach is presented for systematic consideration of the total acquisition duration and placement of scans with the inclusion of the least possible scans, in order to achieve acceptable estimation accuracies for certain perfusion parameters of interest, including the permeability-surface area product.

## MATERIALS AND METHODS

### Tracer Kinetics Model and Perfusion Parameters of Interest

The iodinated contrast medium used in DCE-CT may diffuse from the blood plasma within the capillaries into the tissue interstitial. We employed a two-compartment model which comprised of a vascular compartment and an interstitial compartment, denoted here as compartment 1 and 2, respectively, to account for the intravascular space (IVS) and extravascular, extracellular space (EES). A constant flow rate  $F$  is assumed to supply the IVS, and the tracer kinetics of this bicompartmen-tal tissue system can be described by the following pair of mass-balance equations<sup>13</sup>:

$$v_1 \frac{dC_1(t)}{dt} = -F\rho C_1(t) - K_{21}C_1(t) + K_{12}C_2(t) + F\rho C_a(t) \quad (1a)$$

$$v_2 \frac{dC_2(t)}{dt} = K_{21}C_1(t) - K_{12}C_2(t) \quad (1b)$$

$C_i$  and  $v_i$ , respectively, denote the concentration of contrast medium and fractional volume of the  $i^{\text{th}}$  compartment. The transfer constants for trans-capillary, bidirectional exchange,  $K_{21}$  and  $K_{12}$ , are related to their corresponding rate constants ( $k_{21}$  and  $k_{12}$ ) by  $k_{ij}=K_{ij}/v_j$ .<sup>3</sup>  $\rho$  is the tissue density which is assumed unity in this study.

The impulse residue function  $R(t)$  deduced from Eq. 1(a) and 1(b), takes the biexponential form

$$R(t) = A \exp(\alpha t) + (1 - A) \exp(\beta t), \quad (2)$$

with

$$\alpha = \frac{1}{2} \left[ -\left(k_{21} + k_{12} + \frac{1}{t_1}\right) + \sqrt{\left(k_{21} + k_{12} + \frac{1}{t_1}\right)^2 - 4\frac{k_{12}}{t_1}} \right],$$

$$\beta = \frac{1}{2} \left[ -\left(k_{21} + k_{12} + \frac{1}{t_1}\right) - \sqrt{\left(k_{21} + k_{12} + \frac{1}{t_1}\right)^2 - 4\frac{k_{12}}{t_1}} \right]$$

$$\text{and } A = \frac{\alpha + k_{12} + k_{21}}{\alpha - \beta}.$$

The vascular transit time  $t_1$  is related to  $F$  and  $v_1$  through the central volume relation, i.e.  $v_1 = Ft_1$ .

The tissue concentration curve  $C_{\text{tiss}}(t)$  can be described by

$$C_{\text{tiss}}(t) = F\rho C_a(t) \otimes R(t) \quad (3)$$

where  $\otimes$  denotes the convolution operator and  $C_a(t)$  is the arterial input function sampled from a feeding artery. To derive estimates of the perfusion parameters, Eq. 3 can be optimally fitted against tissue concentration curves extracted from the DCE imaging dataset, by adjusting the parameters  $F$ ,  $v_1$ ,  $k_{21}$ , and  $k_{12}$ . Assuming passive diffusion of contrast medium between the IVS and EES, the permeability-surface area product PS can be obtained by  $PS = k_{21}v_1$ .<sup>14</sup>

As the cancerous tissue could exhibit increased blood flow, vascularity, and permeability, the parameters of interest which we would be focusing on are  $F$ ,  $v_1$ , and PS, and we attempted to study their estimation accuracy for different imaging sequences.

### Monte Carlo Simulations

The Monte Carlo (MC) simulation approach was used to evaluate the accuracy of parameters

derived from different imaging protocols. The simulation experiments were set up in a similar fashion as in the studies of Ostergaard et al. and Calamante et al.<sup>15,16</sup> The simulated arterial input curve was in the form of a gamma density function

$$C_a = \begin{cases} C_0(t - t_0)^a e^{-(t-t_0)/b} & t > t_0 \\ 0 & \text{otherwise} \end{cases}, \quad (4)$$

where the parameters  $C_0$ ,  $t_0$ ,  $a$ , and  $b$  are obtained by fitting an actual arterial input function sampled from a patient study case, as shown in Figure 1.

Using  $R(t)$  and the above simulated  $C_a(t)$ , the tissue concentration curve  $C_{\text{tiss}}(t)$  can be simulated using Eq. 3, by assuming appropriate values for the model parameters  $F$ ,  $v_1$ ,  $k_{21}$ , and  $k_{12}$ . The parameter values used in this study were obtained from a previous study<sup>8</sup> in our institution after institutional review board approval and informed consent from the patients as well as from similar studies in literature.<sup>9–10</sup> These parameter values are  $F=70$  ml/min/100 g,  $v_1=5$  ml/100 g,  $k_{21}=3.4$  min<sup>-1</sup>, and  $k_{12}=0.85$  min<sup>-1</sup>, giving PS=17 ml/min/100 g.

Synthetic dynamic images<sup>15,16</sup> were constructed using the simulated  $C_{\text{tiss}}(t)$  curves with each dataset consisting of  $N$  images of  $32 \times 32$  voxels (i.e. 1,024  $C_{\text{tiss}}(t)$  curves) and with time interval

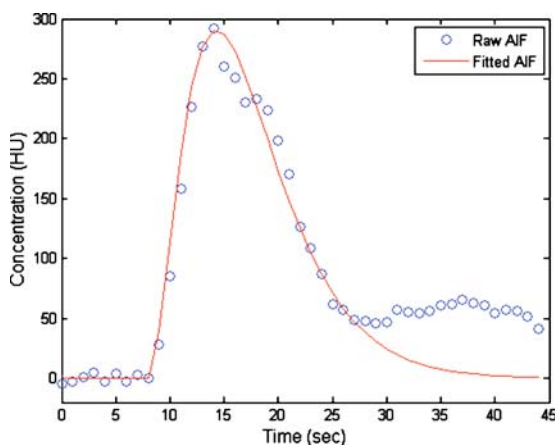


Fig 1. The simulated arterial input function (AIF) used in this study was obtained by fitting the gamma density function in Eq. 4 against an actual AIF (circles) obtained from a previous patient study case. Features related to recirculation in the actual AIF were not fitted and were removed in the fitted gamma density function. The values of the fitted parameters in Eq. 4 are:  $C_0 = 54$ ,  $t_0 = 8$  s,  $a = 2$ , and  $b = 0.32$  s. When used in the subsequent Monte Carlo simulations,  $t_0$  is set to 0 to simulate the bolus arrival at time  $t = 0$ .

$\Delta t$ . In this study, different values of  $N$  and  $\Delta t$  were considered to arrive at an optimal imaging protocol. Gaussian noise was added to the synthetic dynamic images to generate signal-to-noise ratio (SNR) of 10, which are typical of DCE imaging.<sup>15</sup> SNR was taken to be the ratio of the maximum value of  $C_{\text{tiss}}(t)$  (before noise was added) and the standard deviation of noise.<sup>15</sup> In previous works<sup>15</sup>, a preprocessing step of median filtering the synthetic dataset was applied to reduce noise before deconvolution analysis. This was not performed in the present study so that the dataset remain significantly noisy and poses an actual challenge to the parameter estimation process by data fitting. To avoid data fitting problems associated with initial-point dependence and trapping within local minima, the initial fitting parameter values were chosen randomly from within physiological ranges of the parameters, and restarted 10 times. The best fit obtained from the 10 runs was taken as the final fitting for each noisy  $C_{\text{tiss}}(t)$  curve. Due to the random noise added, the final “best fit” to each noisy  $C_{\text{tiss}}(t)$  curve might not correspond to the original  $C_{\text{tiss}}(t)$  curve (see Fig. 2), and the estimated parameters could also deviate from those used to generate the original  $C_{\text{tiss}}(t)$  curve. The % error (or coefficient of variation) of each parameter was calculated using the standard deviation of the estimated parameter from 1024 runs divided by the actual parameter value.

### Simulation Experiments #1

To study the effects of different values of  $N$  and  $\Delta t$  on the estimation accuracy of the parameters  $F$ ,  $v_1$ , and PS, we first performed simulations for  $N=50, 60, 70, 80, 90$ , and 100 scans. For a set of  $N$  images, the scan interval further ranges from  $\Delta t=0.5, 1, 2, 3, 4$ , and 5 s. For a simulation dataset corresponding to a particular value of  $N$  and  $\Delta t$ , the total examination time  $T$  is given by  $T=N\Delta t$ , and the maximum examination duration simulated was 500 s ( $100 \times 5$  s). In all these simulations, the perfusion values assumed were  $F=70$  ml/min/100 g,  $v_1=5$  ml/100 g, and PS=17 ml/min/100 g. This initial set of simulation experiments was aimed at providing insights on the possible changes in the estimation errors of  $F$ ,  $v_1$ , and PS for various values of  $N$ ,  $\Delta t$ , and hence  $T$ . For permeability imaging, it would be interesting to

also explore the effects on parameter estimation due to changes in tissue permeability PS. Thus, we have also performed a set of simulations for  $N=50$  and  $\Delta t=1$  s, with PS varying between 2 to 40 ml/min/100 g, while  $F$  and  $v_1$  were kept constant at 70 ml/min/100 g and 5 ml/100 g, respectively.

### Simulation Experiments #2: A Dual-phase Imaging Protocol

As will be illustrated in the following section, results from simulation experiments #1 suggested that initial scans with short time intervals would allow the first-pass parameters  $F$  and  $v_1$  to be estimated more accurately, while the accuracy for PS would increase with  $N$  and  $T$ . However, an imaging protocol with consistently small  $\Delta t$  and large  $N$  is not feasible due to the increased radiation exposure. In the following, we propose a dual-phase imaging sequence which includes both an initial and delayed imaging phase, in the attempt to estimate all three parameters,  $F$ ,  $v_1$ , and PS accurately.

Suppose a total of  $N$  scans are performed, we allow an initial number of constant-interval scans ( $N_{ICS}$ ) with a fixed interval of  $\Delta t$  to provide accurate estimation of  $F$  and  $v_1$ , while the remaining scans ( $N_{REM}=N-N_{ICS}$ ) are increasingly spaced out, so that data could be collected over a longer period of time. For this reason, we increased the scan interval exponentially using the following form:

$$\Delta t_{VAR} = \Delta t \exp[\alpha i], \quad (5)$$

where  $i = 1, 2 \dots N_{REM}$ ,

such that the time interval between scans is now a variable  $\Delta t_{VAR}$  that increases with each scan after  $N_{ICS}$ . The parameter  $\alpha$  governs the rate of increase in  $\Delta t_{VAR}$ , thus giving us the advantage of increasing the examination duration  $T$ , without increasing  $N$ . As an example, suppose that  $N=50$ ,  $N_{ICS}=10$ ,  $N_{REM}=40$ ,  $\Delta t=1$  s, and  $\alpha=1$ , then the scan times are

$$\begin{aligned} &0, 1 \text{ s}, 2 \text{ s}, 3 \text{ s}, 4 \text{ s}, 5 \text{ s}, 6 \text{ s}, 7 \text{ s}, 8 \text{ s}, 9 \text{ s}, 9 \\ &+ \exp(1), 9 + \exp(1) + \exp(2), \dots 9 \\ &+ \sum_{i=1}^{40} \exp(i) \left[ \text{or } 9 + \Delta t \sum_{i=1}^{N_{REM}} \exp(\alpha i) \right] \end{aligned}$$

and  $T$  now not only depends on  $N$ , but also on  $N_{ICS}$ ,  $\Delta t$ , and  $\alpha$ , as follows

$$T = (N_{ICS} - 1)\Delta t + \Delta t \sum_{i=1}^{N_{REM}} \exp(\alpha i). \quad (6)$$

The problem of finding an optimal imaging protocol is multi-dimensional which involves  $N$ ,  $N_{ICS}$ ,  $\Delta t$ , and  $\alpha$ . We attempted to transform this problem into two subproblems of locating local suboptimal values, which can be systemically approached in the following manner. We first fix  $N$  at the conventionally acceptable value of 50 and study the parameter errors for various values of  $N_{ICS}$  (10, 15, 20, 25, 30, 35, 40),  $\Delta t$  (0.5, 1, 1.5, and 2 s), and  $\alpha$  (0.05, 0.06, 0.07, ..., 0.2). Optimal values of  $N_{ICS}$ ,  $\Delta t$ , and  $\alpha$  (and hence  $T$ ) were manually identified using contour plots of these variables as a function of the perfusion parameter errors. On the basis of the selected optimal values for  $N_{ICS}$ ,  $\Delta t$ , and  $T$ , we then consider decreasing values of  $N$  in the attempt to identify the smallest value of  $N$  that do not compromise on the accuracy of the perfusion parameters. In this set of simulation experiments, the perfusion values assumed were again  $F=70$  ml/min/100 g,  $v_1=5$  ml/100 g, and PS=17 ml/min/100 g.<sup>8</sup>

After defining the optimal scan duration and number of scans, the acquisition protocol was applied in a patient with a head and neck tumor (left parotid gland) after informed consent was obtained. A single 12-mm-thick tumor slab was examined using a 16-row multislice CT scanner (Somatom 16, Siemens Medical Systems, Erlangen, Germany). The contrast agent for perfusion imaging (40 ml of 400 mg/dl nonionic iodinated contrast agent, Imeron 400, Altana, Germany) was injected also at a rate of 5.5 ml/s using a power injector. Perfusion scanning (100 mA, 120 kV) was initiated 6 s after the injection start. The contrast agent administration was followed by a power injection of 20 ml saline at the same injection rate.

## RESULTS

### Simulation Experiments #1

Two examples of fitting the noisy  $C_{tiss}(t)$  curves are shown in Figure 2: for  $N=50$  with  $\Delta t=1$  s and for  $N=100$  with  $\Delta t=5$  s, together with the

corresponding impulse residue functions  $R(t)$  derived. The original simulated  $C_{\text{tiss}}(t)$  and  $R(t)$  curves are also provided for comparison. Figure 2 also serves to illustrate the shape of the simulated  $C_{\text{tiss}}(t)$  curves and to provide a rough idea of the time span in which  $C_{\text{tiss}}(t)$  is significantly nonzero.

Results of the MC simulations for  $N=50, 60, 70, 80, 90,$  and  $100$  scans with a fixed scan interval of  $\Delta t=1$  s are shown in Figure 3a. Figure 3b and c show the simulated error estimates for various values of  $\Delta t$  with the total number of scans kept at  $N=50$  and  $N=100$ , respectively. Figure 3a shows that the estimation errors of all perfusion parameters should decrease with the increase in the number of scans  $N$ , when the scan interval  $\Delta t$  is

kept constant. In this case, we note that PS is most sensitive to the increase in  $N$  (or  $T$  since  $T=N\Delta t$  in this set of experiments), with the reduction of its error from about 20% to 10%; while improvement in errors of  $F$  and  $v_1$  are more obvious when  $N$  is small. Figure 3b and c suggests that the estimation errors of each perfusion parameter could either increase or decrease with the increase of scan interval  $\Delta t$ , depending on the number of scans  $N$ .

Figure 4 shows that when  $N$  and  $\Delta t$  were kept constant at 50 and 1 s, respectively, changes in PS values resulted in different errors not only for the PS parameter but also affected the error of the parameters  $F$  and  $v_1$ , even though the values of  $F$  and  $v_1$  were kept constant. This indicates that in

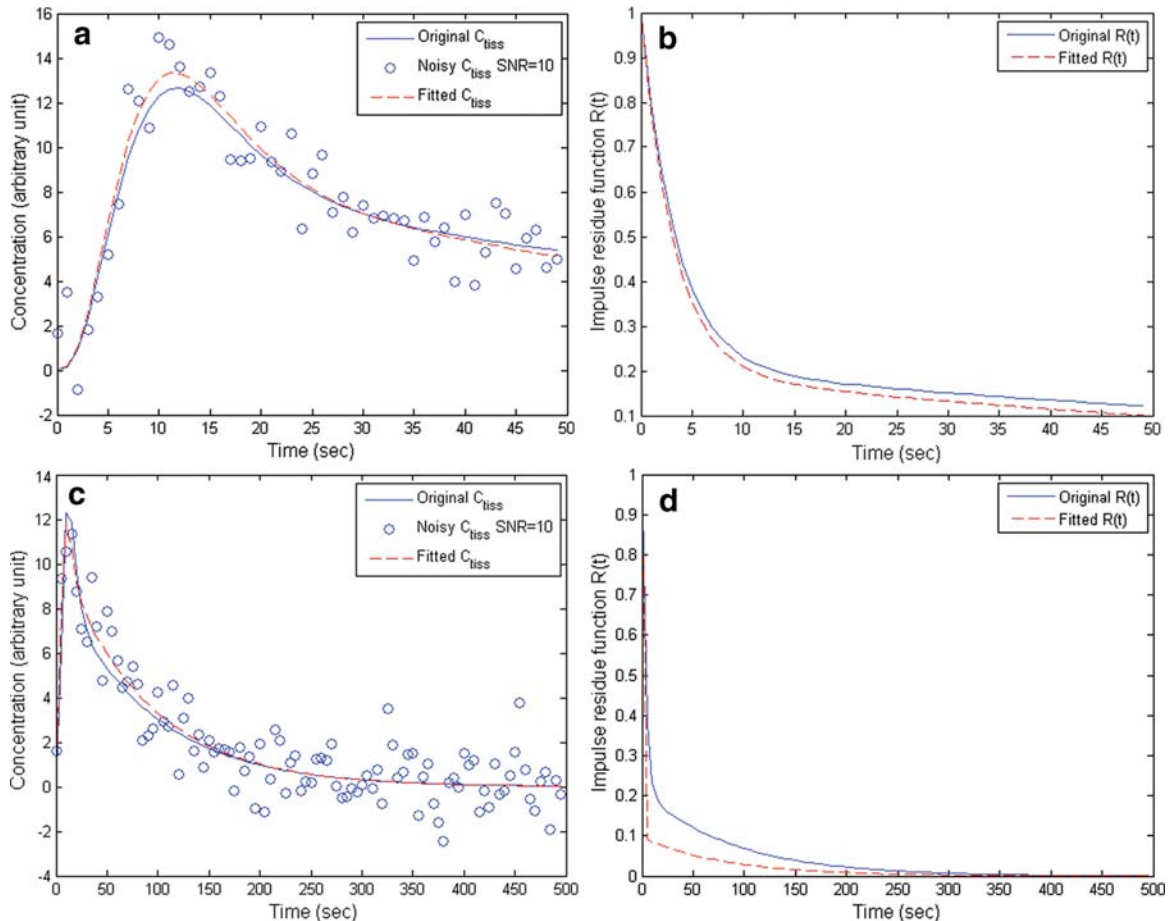


Fig 2. Examples of two simulation runs for  $N=50$  with  $\Delta t=1$  (a, b); and  $N=100$  with  $\Delta t=5$  (c, d). In each case, a noisy  $C_{\text{tiss}}(t)$  is simulated by adding Gaussian noise (SNR = 10) onto a clean  $C_{\text{tiss}}(t)$  curve generated using Eq. 3 (a, c). The noisy  $C_{\text{tiss}}(t)$  then undergoes a fitting process in the attempt to estimate the perfusion parameter values used to generate the original  $C_{\text{tiss}}(t)$ . The original and fitted impulse residue functions  $R(t)$  differ as shown in b and d, resulting in deviations of the estimated perfusion parameters. This process is repeated for 1,024 runs and the standard deviation of each parameter is used as an indication of parameter estimation error.

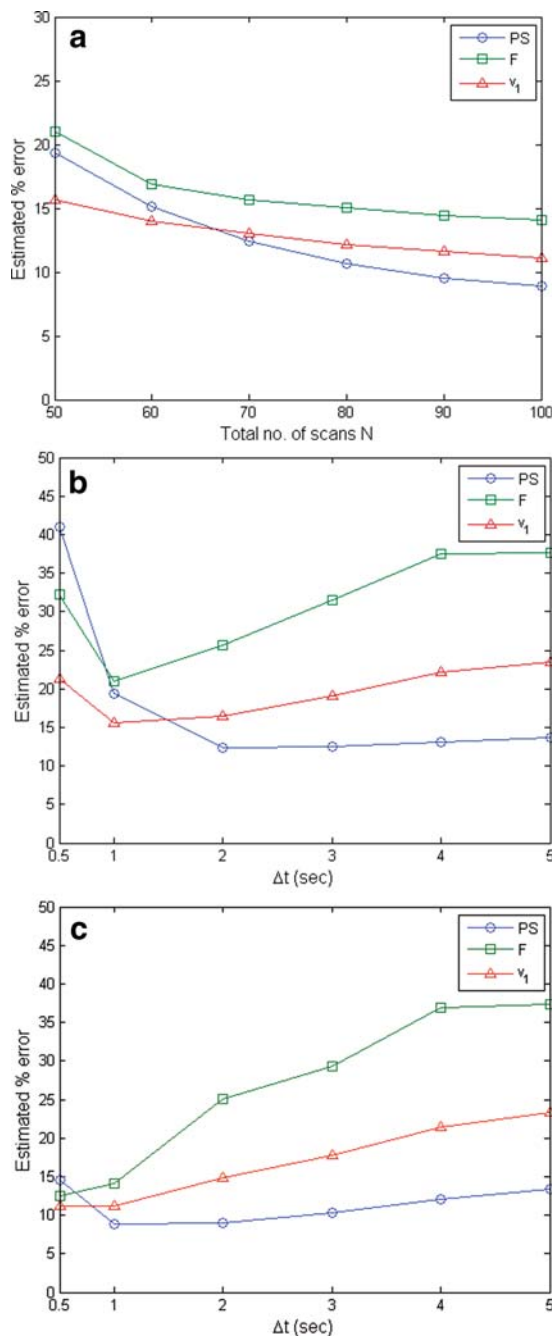


Fig 3. Results of MC simulations for  $N=50, 60, \dots, 100$ , with a constant time interval of  $\Delta t=1$  s (a) and simulation results for various scan intervals  $\Delta t=0.5, 1, \dots, 5$  s for a fixed number of scans  $N=50$  (b) and for  $N=100$  (c). (PS permeability surface area product,  $F$  blood flow,  $v_1$  intravascular blood volume).

cases with highly permeable vasculature, large errors ( $>20\%$ ) in the estimated perfusion values might be expected, if the scan parameters  $N$  and  $\Delta t$  were not appropriately set.

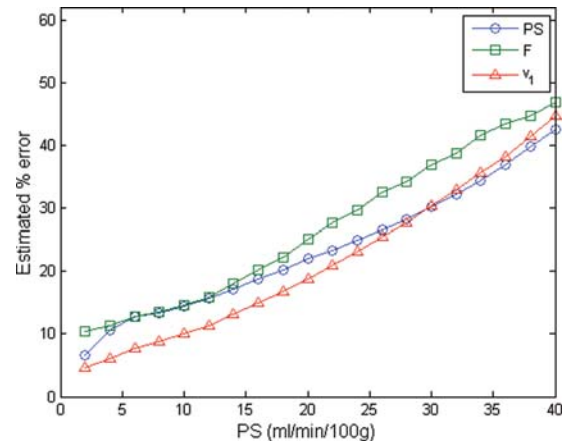


Fig 4. Estimation of the error (in %) of the perfusion parameters in association with the PS values. In these simulations, the scan parameters were fixed at  $N=50$  scans with  $\Delta t=1$  s and the values of  $F$  and  $v_1$  were kept constant at 70 ml/min/100 g and 5 ml/100 g, respectively, while PS changes from 2 to 40 ml/min/100 g. The results show that with  $N=50$  scans and  $\Delta t=1$  s, there could be marked increase in the estimated errors for all perfusion parameters, with the increase in PS, which can be associated with highly permeable tumor tissue. (PS permeability surface area product,  $F$  blood flow,  $v_1$  intravascular blood volume).

### Simulation Experiments #2: A Dual-phase Imaging Protocol

With  $N=50$ , and for various values of  $N_{ICS}$  ( $=10, 15, \dots, 40$ ),  $\Delta t$  ( $=0.5, 1, \dots, 2$  s), and  $\alpha$  ( $=0.05, 0.06, \dots, 0.2$ ), a large amount of simulation data was generated, and Figure 5 attempts to summarize these results in the form of contour plots. Each of the three rows corresponds to a particular perfusion parameter and each of the four columns refers to a fixed value of  $\Delta t$ . Within each contour plot, various values of  $N_{ICS}$  and  $\alpha$  were displayed. The contour lines and values in each contour plot refer to the % error of the corresponding perfusion parameter. For example, the plot in the row 1, column 1 shows that the error in  $F$  ranges from about 14% to 28% when  $\Delta t=0.5$  s, and for various values of  $N_{ICS}$  and  $\alpha$ .

Along the rows as  $\Delta t$  increases from 0.5 to 2 s, the range of errors for  $F$  and  $v_1$  generally increases, while the error range for PS decreases, which is consistent with the observation that shorter time intervals are preferred for the estimation of  $F$  and  $v_1$ , and vice versa for PS. An optimal point along each column is identified by considering the contours of  $F$ ,  $v_1$ , and PS for each  $\Delta t$ . Each optimal point is marked with a marker (circle,

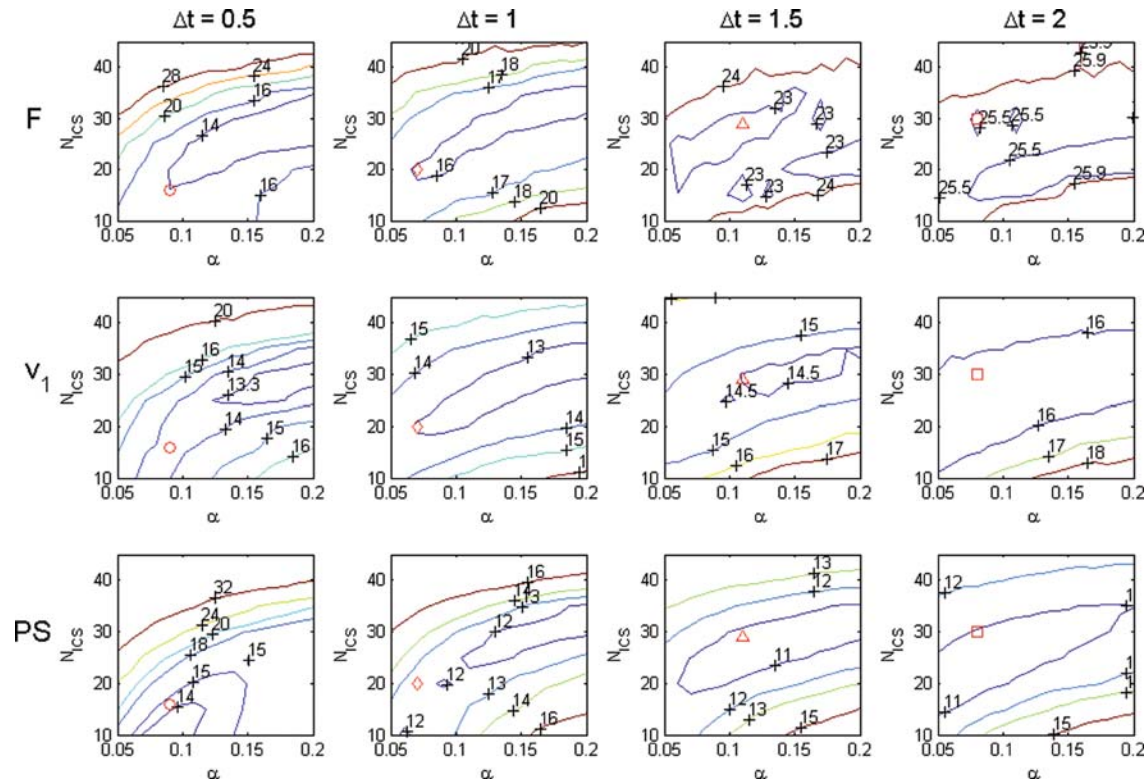


Fig 5. Contour plots of the estimated error in the perfusion parameters generated with a fixed number of scans  $N = 50$ , and for various values of  $\Delta t = 0.5, 1, 1.5, 2$  s, number of initial scans with constant interval  $N_{ICS} = 10, 15, 20, 25, 30, 35, 40$  and  $\alpha = 0.05, 0.06, 0.07, \dots, 0.2$  (see [Materials and Methods](#)).

diamond, triangle, and square) and denotes a set of values for  $N_{ICS}$  and  $\alpha$  (and hence  $T$ ). Considerations for choosing the optimal points include: (1) compromise of minimal error between all three perfusion parameters and (2) small  $\alpha$  values are preferred so that the final scan time is not delayed for too long (e.g., for  $\alpha=0.2$ , the last scan could reach 1 h).

Only the first two optimal points in Figure 5 (i.e. circle marker:  $\Delta t=0.5$  s,  $N_{ICS}=15$ ,  $\alpha=0.09$ , and diamond marker:  $\Delta t=1$  s,  $N_{ICS}=20$ ,  $\alpha=0.07$ ) were further investigated in Figure 6, because the errors for  $F$  and  $v_1$  for the other two optimal points (corresponding to  $\Delta t=1.5$  and 2 s) are significantly larger. Consistently for the first two optimal points, the examination duration  $T$  was about 150 s (Eq. 6). Based on the first two optimal points, Figure 6 further illustrates the effect of reducing the total number of scans  $N$ , with the examination duration  $T$  kept at 150 s. Since the scan timings are calculated using an exponential function (Eq. 5), they may not be integer values in

terms of seconds. For practical implementation of the scans, simulations were also carried out with the scan timings rounded to the nearest integer values in seconds. These results are also shown in Figure 6.

## DISCUSSION

### Simulation Experiments #1

The parameter  $F$  acts like a scaling factor in Eq. 3 and affects the entire  $C_{tiss}(t)$  curve (i.e. both the rising and decreasing portions), while  $v_1$  is dependent on the area under the  $C_{tiss}(t)$  curve (when the tracer leaks, the area under  $C_{tiss}(t)$  curve should be, strictly speaking, equal to the sum of  $v_1$  and the interstitial space reachable by the tracer). Thus, these parameters could be well-estimated if a sufficient portion of the  $C_{tiss}(t)$  curve can be captured, as in Figure 2a, where  $\Delta t=1$  s and the 50 scans cover up to 49 s. However, a temporal

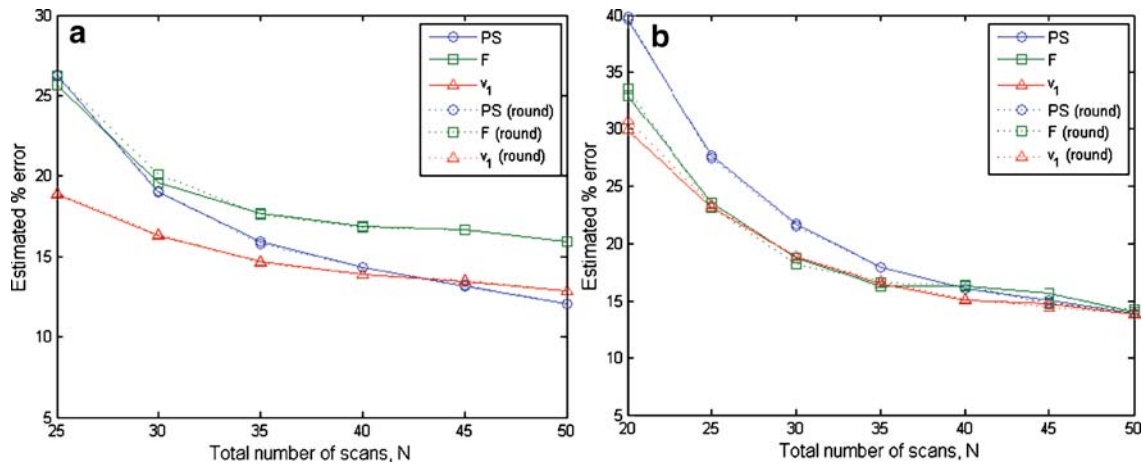


Fig 6. Corresponding to the first two optimal points identified in Figure 5, the total number of scans is now reduced from  $N = 50, 45, 40, 35, 30, 25, 20$ , for  $\Delta t = 0.5$  s,  $N_{ICS} = 15$  (a) and for  $\Delta t = 1$  s,  $N_{ICS} = 20$  (b). In all cases, the examination duration  $T$  is kept at 150 s by solving for appropriate values of  $\alpha$  using Eq. 6. The respective dotted lines indicate the corresponding simulations with the scan timings rounded to the nearest integer value in seconds. These results show that the most acceptable solutions are yielded with a total of about 40 to 50 scans, and that for practical implementation of the scans, rounding the scan timings to the nearest second would not significantly affect estimation error of the perfusion parameters.

resolution of  $\Delta t = 0.5$  s resulted in 50 scans concentrated only in the initial 24.5 s, which may not provide adequate information on the  $C_{tiss}(t)$  curve to estimate both  $F$  and  $v_1$  accurately. The increase from  $\Delta t = 0.5$  s to  $\Delta t = 1$  s led to a decrease of the errors for  $F$  and  $v_1$ , before increasing with further increase in  $\Delta t$ . This is likely due to the interplay of two factors: (1) temporal resolution  $\Delta t$ , and (2) total examination duration  $T$ . When the examination duration  $T$  allows for sufficient coverage of the  $C_{tiss}(t)$  curve, the importance of time resolution takes major effect in affecting estimation errors. The AIF (see Fig. 1) typically spans about 20–30 s (depending on the injection rate), and for a larger  $\Delta t$ , the AIF is only represented by a few nonzero points. This inadequate representation of the AIF could also contribute to the estimation errors of  $F$  and  $v_1$ . Furthermore, as illustrated in Figure 2c where  $N = 100$  and  $\Delta t = 5$  s, later scans ( $\sim 200$  s onwards) might not be able to provide additional information in estimating  $F$  and  $v_1$  as the  $C_{tiss}(t)$  curve flattens and noise dominates.

The parameter PS governs the later portion of the  $C_{tiss}(t)$  curve, and its optimal estimation is dependent on sufficient coverage of the decreasing portion of the  $C_{tiss}(t)$  curve, without excessive delayed imaging that will result in the sampling of near-zero  $C_{tiss}(t)$  points and the inadequate sampling of the AIF. Hence, minimal error for PS

occurs around  $\Delta t = 2$  s in Figure 3b. An interesting finding of this study was that the increase in PS could result in the increase of its own estimation error when the scan parameters are fixed at  $N = 50$  and  $\Delta t = 1$  s (Fig. 4). The increase in the error of PS is likely due to the fact that longer examination duration would be desirable for the estimation of higher PS values. It is interesting to note that these results also indicate a confounding effect between the perfusion parameters as the error in estimating PS during curve fitting can also affect the estimation of the other parameters.

### Simulation Experiments #2: A Dual-phase Imaging Protocol

For the first two optimal points identified in Figure 5, the examination duration  $T$  was found to be about 150 s. This is again consistent with the above observations on the useful portion of the  $C_{tiss}(t)$  curve in the presence of noise. For a constant examination duration of 150 s, Figure 6 shows that a dual-phase imaging sequence of  $N = 40$  to 50 scans, with  $[\Delta t = 0.5$  s,  $N_{ICS} = 15]$  or  $[\Delta t = 1$  s,  $N_{ICS} = 20]$  might yield acceptable estimation errors for all three perfusion parameters. As an example for an exponentially spaced sequence and rounded scan timings for practical implementation, consider the case of  $[\Delta t = 0.5$  s,  $N_{ICS} = 15]$ , the scan timings in seconds for 45 scans are: 0, 0.5, 1, 1.5,

2, 2.5, 3, 3.5, 4, 4.5, 5, 5.5, 6, 6.5, 7, 7.6 (rounded to 8), 8.2(8), 8.9(9), 9.7(10), 10.6(11), 11.6(12), 12.8(13), 13.9(14), 15.4(15), 16.9(17), 18.8(19), 20.8(21), 23.0(23), 25.6(26), 28.4(28), 31.6(32), 35.2(35), 39.2(39), 43.7(44), 48.8(49), 54.5(55), 60.9(61), 68.0(68), 76.1(76), 85.1(85), 95.3(95), 106.7(107), 119.5(120), 133.9(134), and 150. Here, we note that since two scans are rounded to 8 s, there are only 44 scans when implemented practically. Figure 7 shows the parametric color-coded perfusion maps of the examined patient and the histogram analysis of the acquired perfusion values using our optimized perfusion CT protocol.

### Clinical Implications

The two primary issues with multislice CT imaging are speed and organ coverage. The new multidetector CT scanners can achieve very short rotation time of about 0.3 s (implemented in heart CT protocols) but when performing a perfusion study, rotation time of 0.75–1 s is acceptable and

coverage—imaging the entire organ—is the next important issue. As coverage increases with the new CT scanners, the beam collimation and the use of different number of detectors may also be variably changed in order to achieve the desired coverage or reconstruction. The difference in beam collimation, not the reconstructed section width, makes a significant difference in the radiation dose with the higher doses coming from narrower beam collimation. Maximum organ coverage and optimal temporal resolution balanced with acceptable radiation burden are the cornerstones of the optimal perfusion imaging.

While an initial evaluation of optimal scan duration in cerebral CT perfusion studies of patients with cerebrovascular disease has already been reported<sup>17</sup>, tumor perfusion imaging which includes permeability imaging has not been systematically investigated, apart from some initial remarks in colorectal cancer imaging.<sup>11,18</sup> Although the estimation of the CT-based first-pass tracer kinetic parameters like  $F$  in extracranial head

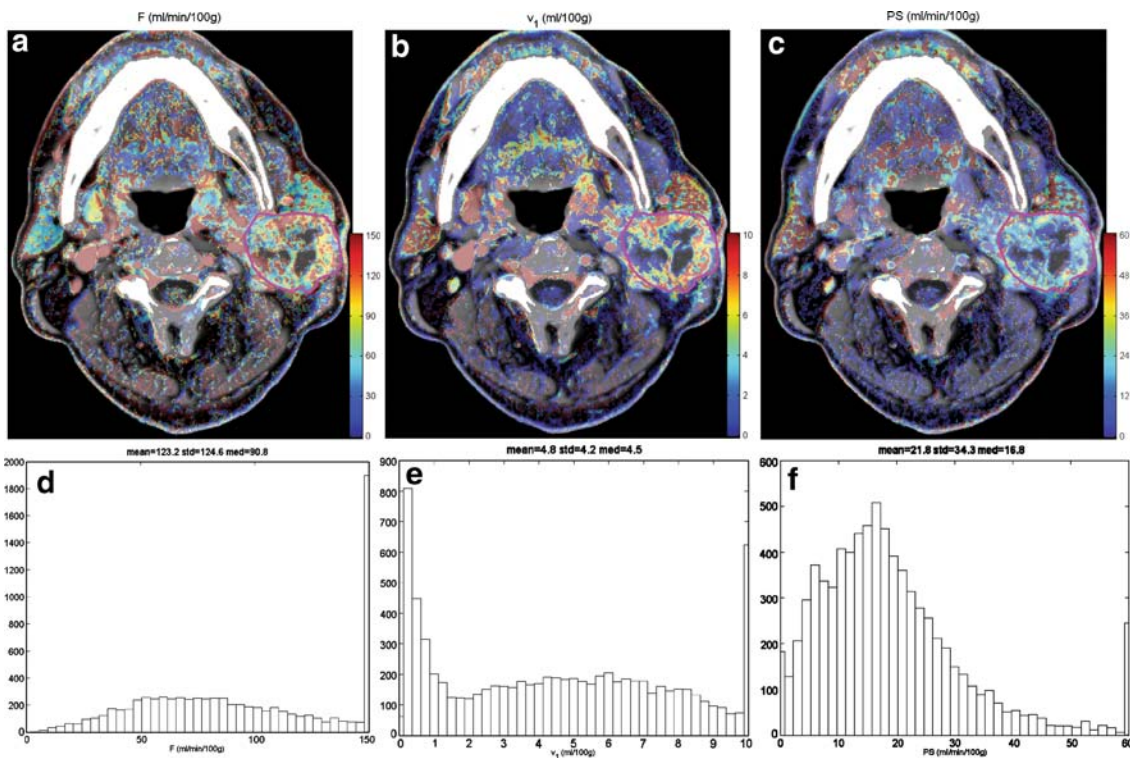


Fig. 7. Parametric maps of a blood flow  $F$ , b blood volume  $v_1$ , and c permeability-surface area product  $PS$  for a patient study case (left parotid gland adenocarcinoma). Tumor outlines are shown in magenta. Histograms corresponding to d blood flow  $F$ , e blood volume  $v_1$ , and f permeability-surface area product  $PS$  within the outlined tumor are also shown.

and neck tumors has not been validated using a gold standard like radio-labeled  $H_2O$  positron emission tomography (PET) imaging, the derived functional values in the initial studies<sup>8-10</sup> (which were the input parameter in our protocol) appear consistent with the tumor physiology in terms of increased cell proliferation and neoangiogenesis in order to satisfy the increased demand in blood supply. These phenomena result in elevated blood flow  $F$  (multiple abnormal low-resistance shunts of the newly formed vessels where the blood rapidly flows), elevated blood volume  $v_1$  (as a measure of the tumor vasculature), and increased permeability-surface area product PS (due to immature newly formed vessels with increased fenestration which results in rapid extravasation of the contrast agent into the interstitial extracellular space). Accurate quantification of the perfusion parameters would have important applications, besides the tumor diagnosis<sup>8</sup>, in both pharmaceutical and clinical trials as these parameters are important noninvasive surrogates of tumor activity, tumor response to treatment, and tumor growth prediction.

One common hypothesis in order to reduce the radiation dose is to reduce the number of scans within a certain scanning time, to reduce the scanning time, or modify the acquisition parameters (beam energy, tube current-time product, collimation) but such approaches may result in large deviations from the validated perfusion values.<sup>19</sup> In our study, we attempted to optimize the DCE-CT (or perfusion) protocol only in terms of temporal resolution and number of scans in order to derive the lowest possible estimation error of the calculated perfusion parameters including permeability imaging. Due to radiation safety issues, an optimization by means of randomized DCE-CT studies protocols in different patient populations is not allowed and, therefore, we chose to perform Monte Carlo simulations. Our results suggest that a practical and appropriate protocol may consist of two components (or imaging phases): (a) an initial number of 15 constant-interval scans ( $\Delta t=0.5$  s), so as to ensure good estimation of  $F$  and  $v_1$  in the first pass of the contrast agent and (b) a number of subsequent scans with increasing intervals in-between to capture capillary-tissue exchange processes.

A confounding effect between the perfusion parameters was observed in our work. The fact that the perfusion parameters are interdependent on

each other's estimation/error implies that the application of a universal perfusion CT protocol for all tumors may not be realistic. In other words, remarkably different PS values (or different  $F$  and  $v_1$  values) resulting from different tumor histological types and tumor microenvironment can lead to false estimations of the other perfusion parameters if we rely on a globally standardized DCE-CT protocol.<sup>20</sup> Whether these errors could pose clinical significance that may lead to false perfusion-based diagnosis or therapy monitoring is questionable, and this may be of interest for future investigation.

The radiation dose and the patient discomfort due to long examination time are two major drawbacks in the attempt to gain more functional information that will result to a better understanding of the examined organ. In our patients<sup>8</sup>, a decreased tube current and peak kilovoltage (100 mAs, 120 kVp) compared to the initially reported perfusion CT studies<sup>21</sup> led to a reduced radiation burden. Nevertheless, there may be still some space for further reduction of the tube voltage as lower tube voltage, theoretically increasing the image noise but in a smaller magnitude in smaller structures (i.e. neck) compared to larger sized structures (i.e. abdomen), enhances the contrast-to-noise ratio and the image contrast after iodine administration.<sup>22</sup> Murase et al. have drawn attention in this issue by showing that large variations from established perfusion values can appear<sup>19</sup> if acquisition parameters are significantly modified. According to Hamberg et al.<sup>23</sup>, the weighted CT dose index ( $CTDI_{100w}$ ) of a multi-slice CT scanner (Lightspeed QX/i, GE Medical Systems) is  $6.2 \pm 0.2$  mGy when using the following parameters: tube settings of 80 kVp and 100 mAs, four 5-mm-thick contiguous slices, and tube rotation time of 1 s. Assuming that there is a linear relationship between tube current and rotation time and radiation dose, an almost linear relationship between tube voltage and radiation dose, it is easy to determine that the dose in our protocol (45 scans and 0.5 s rotation time in body mode) is substantially lower than that of a head perfusion study (200 mAs, 80 kV, 1 s rotation time) with the same slices and number of scans. More accurately, the calculation of the mean effective dose in the patient population<sup>8</sup> based on the dose length product (55 s acquisition duration, 1 image/s) and the conversion factor for neck<sup>24</sup> showed a mean effective dose of 8.8 mSv which is

supposed to be reduced in the optimized protocol of 45 image acquisitions. The possible reduction of the necessary scans may enable the radiologist to perform two subsequent perfusion surveys in order to cover the whole extent of the tumor. It was beyond the scope of this study to determine if other acquisition parameters would provide lower radiation burden given the same image quality.

One limitation of our study is its application in head and neck tumors. Other tumor histologies in various organs with different perfusion properties could result in wider or narrower  $C_{\text{tiss}}(t)$  curves, and hence the present recommended imaging protocol might not be suitable. Also, if the injection rate is much higher or lower, the width of the AIF would be different, which can affect the relationship between estimation errors and sampling time resolution. However, the considerations and approach put forward here in choosing an optimal protocol can still be adopted, if appropriately translated to account for these differences.

Our work is distinctive in that, though perfusion analysis is commercially available from major CT vendors (e.g. General Electric, Mi, WI or Siemens Medical Solutions, Erlangen, Germany) through ready-made for analysis of DCE images packages, these software packages may not be amenable to performing Monte Carlo simulation studies, and the present simulation studies have been performed using Matlab™ (MathWorks, Natick, MA, USA) programs which are developed in-house. Nevertheless, the first scans with 0.5 s constant interval are not difficult to put into practice in the era of the 32- and 64-slices CT scanners. The rounded values of the exponentially calculated scan timings can be easily implemented in the scan protocols and as shown in Figures 6 and 7, the results are not significantly different from the original exponential scan timings and the known perfusion maps, respectively. Moreover, the perfusion software provided by Siemens is based on the maximum slope model with Patlak analysis for the calculation of the extravasation parameters. These tracer kinetic analyses are distinct from the deconvolution-based analysis with the adiabatic tissue homogeneity model for calculation of the PS (used in the GE software)<sup>25</sup> and the CC approach applied in our tracer kinetic analysis.

Future clinical implications of our work may include standardization of the perfusion CT protocol that might be useful for multicentric studies as well

as for the comparison of studies performed in different institutions. Re-evaluating the importance of reliably estimated PS values in the quantification of neoangiogenesis and its therapeutic monitoring, may have important implications in the discrimination between benign and malignant neoplasms as well as for differentiation between post-therapeutic changes and tumor recurrence in the head and neck tumor patients after (neo)-adjuvant chemo/irradiation (the latter has been proved to be problematic according to a recent study following a 55-s protocol with 1 s constant interval<sup>8</sup>). Our study may be a good starting point in the perfusion protocol optimization in DCE-MR imaging, although, there are other factors specific to MRI like the nonlinear relationship between signal intensity and contrast concentration, the applied sequence and field strength, which could be taken into consideration.

In conclusion, we proposed a method for optimizing the positioning of scans in head and neck tumor perfusion studies, with considerations of reducing radiation dose while maintaining accuracy of the perfusion parameters estimated. The suggested optimized protocols achieved measurements of the permeability surface area product, blood flow, and blood volume with a radiation burden and exam duration balanced estimation error. These optimized protocols can potentially be useful in the clinical setting of examining patients with extracranial head and neck tumors.

#### ACKNOWLEDGEMENTS

The authors acknowledge support from the Singapore Cancer Syndicate (SCS-CS-0072).

#### REFERENCES

1. Lee TY: Functional CT: physiological models. *Trends Biotech* 20:S3–S10, 2002
2. Miles KA: Functional computed tomography. *Eur J Radiol* 38:2079–2084, 2002
3. Tofts PS, Brix G, Buckley DL, et al: Estimating kinetic parameters from dynamic contrast-enhanced T1-weighted MRI of a diffusible tracer: standardized quantities and symbols. *JMRI* 10:223–232, 1999
4. Sobol WT, Cure JK: Can in vivo assessment of tissue hemodynamics with dynamic contrast-enhanced CT be used in the diagnosis of tumors and monitoring of cancer therapy outcomes. *Radiology* 232:631–632, 2004
5. Roberts HC, Roberts TPL, Bollen AW, et al: Correlation of microvascular permeability derived from dynamic contrast-

- enhanced MR imaging with histologic grade and tumor labeling index: a study in human brain tumors. *Acad Radiol* 8:384–391, 2001
6. Lüdemann L, Grieger W, Wurm R, et al: Comparison of dynamic contrast-enhanced MRI with WHO tumor grading for gliomas. *Eur Radiol* 11:1231–1241, 2001
  7. Mayr NA, Hawighorst H, Yuh WTC, et al: MR microcirculation assessment in cervical cancer: correlations with histomorphological tumor markers and clinical outcome. *JMRI* 10:267–276, 1999
  8. Bisdas S, Baghi M, Smolarz A, et al: Quantitative measurements of perfusion and permeability of oropharyngeal and oral cavity cancer, recurrent disease, and associated lymph nodes using dynamic first pass contrast-enhanced computed tomography. *Invest Radiol* 42:172–179, 2007
  9. Rumboldt Z, Al-Okaili R, Deveikis JP: Perfusion CT for head and neck tumors: pilot study. *Am J Neuroradiol* 26:1178–1185, 2005
  10. Gandhi D, Hoeffner EG, Carlos RC, et al: Computed tomography perfusion of squamous cell carcinoma of the upper aerodigestive tract. Initial results. *J Comput Assist Tomogr* 27:687–693, 2003
  11. Goh V, Halligan S, Hugill JA, et al: Quantitative colorectal cancer perfusion measurement using dynamic contrast-enhanced, multidetector-row computed tomography: effect of acquisition time and implications for protocols. *J Comput Assist Tomogr* 29:59–63, 2005
  12. Cenic A, Nabavi DG, Craen RA, et al: A CT method to measure hemodynamics in brain tumors: validation and application of cerebral blood flow maps. *Am J Neuroradiol* 21:462–470, 2000
  13. Brix G, Kiessling F, Lucht R, et al: Microcirculation and microvasculature in breast tumors: pharmacokinetic analysis of dynamic MR image series. *Magn Reson Med* 52:420–429, 2004
  14. Cheong LHD, Lim CCT, Koh TS: Dynamic contrast-enhanced CT of intracranial meningioma: comparison of distributed and compartmental tracer kinetic models—initial results. *Radiology* 232:921–930, 2004
  15. Ostergaard L, Weisskoff RM, Chesler DA, et al: High resolution measurement of cerebral blood flow using intravascular tracer bolus passages. Part I: Mathematical approach and statistical analysis. *Magn Reson Med* 36:715–725, 1996
  16. Calamante F, Cadian D, Connelly A: Quantification of perfusion using bolus tracking magnetic resonance imaging in stroke: assumptions, limitations and potential implications for clinical use. *Stroke* 3:1146–1151, 2002
  17. Hirata M, Sugawara Y, Murase K, et al: Evaluation of optimal scan duration and end time in cerebral CT perfusion study. *Radiat Med* 23:351–363, 2005
  18. Kalra MK, Small WC, Torres WE: A 45-second CT perfusion protocol for rectal cancers may not be adequate to infer vascular permeability-surface area products. *Radiology* 238:755–756, 2006
  19. Murase K, Nanjo T, Li S, et al: Effect of X-ray tube current on the accuracy of cerebral perfusion parameters obtained by CT perfusion studies. *Phys Med Biol* 50:5019–5029, 2005
  20. Fukumura D, Yuan F, Monsky WL, Chen Y, Jain RK: Effect of host microenvironment on the microcirculation of human colon adenocarcinoma. *Am J Pathol* 151:679–688, 1997
  21. Hermans R, Meijerink M, Van den Bogaert W: Tumor perfusion rate determined noninvasively by dynamic computed tomography predicts outcome in head-and-neck cancer after radiotherapy. *Int J Radiat Oncol Biol Phys* 57:1351–1356, 2003
  22. Siegel MJ, Schmidt B, Bradley D, Suess C, Hildebolt C: Radiation dose and image quality in pediatric CT: effect of technical factors and phantom size and shape. *Radiology* 233:515–522, 2004
  23. Hamberg LM, Rhea JT, Hunter GJ, et al: Multi-detector row CT: radiation dose characteristics. *Radiology* 226:762–772, 2003
  24. European Guidelines on Quality Criteria for Computed Tomography (EUR 16262 EN, May 1999). Available at: [www.dr.dk/guidelines/ct/quality/index.htm](http://www.dr.dk/guidelines/ct/quality/index.htm). Accessed February 2008
  25. Goh V, Halligan S, Bartram CI: Quantitative tumor perfusion assessment with multidetector CT: are measurements from two commercial software packages interchangeable. *Radiology* 242:777–782, 2007